High-resolution study of the Gamow-Teller (GT$_-$) strength in the ^{64}Zn(^{3}He, t)^{64}Ga reaction

F. Diel,[1,*] Y. Fujita,[2,3,†] H. Fujita,[3] F. Cappuzzello,[4,5] E. Ganioğlu,[6] E.-W. Grewe,[7] T. Hashimoto,[3] K. Hatanaka,[3] M. Honma,[8] T. Itoh,[3] J. Jolie,[1] Bin Liu,[3] T. Otsuka,[9] K. Takahisa,[3] G. Susoy,[6] B. Rubio,[10] and A. Tamii[3]

[1]*Institut für Kernphysik, Universität zu Köln, D-50937 Cologne, Germany*
[2]*Department of Physics, Osaka University, Toyonaka, Osaka 560-0043, Japan*
[3]*Research Center for Nuclear Physics, Osaka University, Ibaraki, Osaka 567-0047, Japan*
[4]*Istituto Nazionale di Fisica Nucleare, Laboratori Nazionali del Sud, I-95125 Catania, Italy*
[5]*Dipartimento di Fisica e Astronomia, Universitá di Catania, I-95125 Catania, Italy*
[6]*Department of Physics, Istanbul University, Istanbul 34134, Turkey*
[7]*Institut fur Kernphysik, Westfälische Wilhelms-Universität Münster, Germany*
[8]*Center for Mathematical Science, University of Aizu, Aizu-Wakamatsu, Fukushima 965-8580, Japan*
[9]*Department of Physics, University of Tokyo, Hongo, Bunkyo, Tokyo 113-0033, Japan*
[10]*Instituto de Física Corpuscular, CSIC-Universidad de Valencia, E-46071 Valencia, Spain*

(Received 22 January 2018; revised manuscript received 22 March 2019; published 21 May 2019; corrected 4 June 2019)

Gamow-Teller (GT) transitions starting from the $T_z = +2$ nucleus ^{64}Zn to the $T_z = +1$ nucleus ^{64}Ga were studied in a (p, n)-type (^{3}He,t) charge-exchange reaction at a beam energy of 140 MeV/nucleon and scattering angles close to 0°. Here, T_z is the z component of the isospin T. The experiment was conducted at the Research Center for Nuclear Physics (RCNP) in Osaka, Japan. An energy resolution of ≈34 keV was achieved by applying beam matching techniques to the Grand Raiden magnetic spectrometer system. With our good resolution, we could observe GT strength fragmented in many states up to an excitation energy of ≈11 MeV. By performing angular distribution analysis, we could identify states in ^{64}Ga excited by GT transitions. The reduced GT transition strengths [B(GT) values] were calculated assuming the proportionality between the cross sections and the B(GT) values. Shell-model calculations using the GXPF1J interaction reproduced the B(GT) strength distribution throughout the spectrum. States with isospin $T = 3$ were identified by comparing the ^{64}Zn(^{3}He,t)^{64}Ga spectrum with a ^{64}Zn(d, ^{2}He)^{64}Cu spectrum. Relative excitation energies of the corresponding structures are in good agreement, supporting the robustness of isospin symmetry in the mass number $A = 64$ nuclei.

DOI: 10.1103/PhysRevC.99.054322

I. INTRODUCTION

Gamow-Teller (GT) transitions in β decay are mediated by the spin-isospin type $\sigma\tau$ operator and the states excited by them will be called GT states throughout this article [1,2]. The transitions are characterized by spin-isospin flip ($\Delta \boldsymbol{S} = 1$ and $\Delta \boldsymbol{T} = 1$) and no angular momentum transfer ($\Delta \boldsymbol{L} = 0$). In addition, the z component of the isospin T_z [$T_z = (N - Z)/2$] is changed by one unit ($\Delta T_z = \pm 1$). Experimentally, GT transitions are studied in β decays and also in charge-exchange (CE) reactions. While β decays provide direct access to the B(GT) strength through the measurements of partial half-lives and the decay Q values, the attainable transitions are limited. The CE reactions, on the other hand, can selectively excite GT states up to high excitation energies (E_x) [3]. In CE reactions, GT transitions become prominent at scattering angles close to 0° and intermediate beam energies ($E_b > 100$ MeV/nucleon). Under these conditions, there exists a close proportionality between the B(GT) values and the differential GT cross sections [3,4]

$$\frac{d\sigma_{\mathrm{GT}}}{d\Omega}(q,\omega) \simeq K(\omega) N_{\sigma\tau} |J_{\sigma\tau}(q)|^2 B(\mathrm{GT}) \quad (1)$$

$$= \hat{\sigma}_{\mathrm{GT}} F(q,\omega) B(\mathrm{GT}), \quad (2)$$

where $J_{\sigma\tau}(q)$ is the volume integral of the effective interaction $V_{\sigma\tau}$ at momentum transfer q (≈ 0), and $K(\omega)$ is the kinematic factor. In this notation, ω is the total excitation energy of the states in the final nucleus and can be expressed as $\omega = E_x - Q_{\mathrm{g.s.}}$, where $Q_{\mathrm{g.s.}}$ is the Q value of the ground state (g.s.) to ground state transition. The factor $N_{\sigma\tau}$ is a distortion factor and $\hat{\sigma}_{\mathrm{GT}}$ is the unit GT cross section. $F(q,\omega)$ describes the momentum and energy transfer dependence of the GT cross section. At $q = \omega = 0$, $F(q,\omega)$ is unity and $F(q,\omega)$ decreases with ω. The ω dependence of $F(q,\omega)$ can be calculated by distorted-wave Born approximation (DWBA) calculations [3].

Owing to the simplicity of the relationship given by Eqs. (1) and (2), the GT strengths can be studied up to high excitation energies using CE type reactions such as (p, n) and (^{3}He,t). In recent (^{3}He,t) experiments [2], the energy resolution has increased by about one-order-of-magnitude compared to pioneering (p, n) reactions reported in Ref. [5].

*fdiel@ikp.uni-koeln.de
†fujita@rcnp.osaka-u.ac.jp

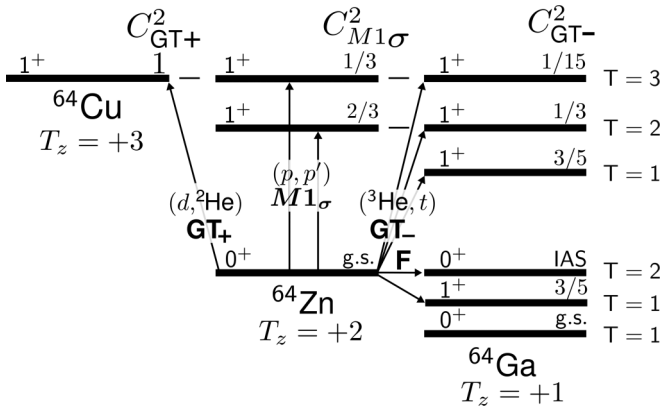

FIG. 1. Schematic isospin structure of $A = 64$ nuclei. J^π values are given for the relevant states. The isospin values T of analog states are shown on the rightmost side. The isospin Clebsch-Gordon coefficients (C^2_{GT}) are written for each transition. Note that the ^{64}Zn g.s. to ^{64}Ga g.s. transition is forbidden due to the GT and Fermi (F) selection rules.

These high-resolution experiments are performed at the Research Center for Nuclear Physics (RCNP), Osaka. The high-resolution facility RCNP offers optimal conditions for the study of GT transition in CE reactions. By the application of beam matching techniques [6,7] to the RCNP spectrometer system, an energy resolution of ≈30 keV can be achieved at an incoming beam energy of $E_b = 140$ MeV/nucleon. A high energy-resolution is crucial for the study of individual GT transitions because the level density especially in the high E_x region can be large.

Here, we studied the GT transitions starting from the pf shell $T_z = +2$ nucleus ^{64}Zn. The GT transitions starting from ^{64}Zn with g.s. T value of 2 are of interest because ^{64}Zn is the heaviest stable nucleus with $T_z = +2$. In addition, GT transitions starting from pf shell nuclei play an important role in the nuclear synthesis of heavy elements (rp process) as well as in the core-collapse process of Type II supernovae [8].

Owing to the $\Delta T = 1$ nature of the $\sigma\tau$ operator, the GT transitions excite states with isospin $T = 1$, 2, and 3 in the final nucleus ^{64}Ga (see Fig. 1). The GT strength distributions of these final T values are overlapping in the spectrum and, therefore, an identification of the isospin value T of the individual states is difficult. Shell-model (SM) [9] calculations using the GXPF1J [10–12] interaction reproduce the general behavior of the GT structure and give valuable insight into the GT strength distributions for the three final T values.

The GT transitions starting from various $T_z = +2$ pf-shell nuclei (^{44}Ca [13], ^{48}Ti [14], ^{52}Cr [15], ^{56}Fe [16], ^{60}Ni [17]) have been studied by the (^{3}He,t) reaction. In the ^{44}Ca(^{3}He,t)^{44}Sc and ^{48}Ti(^{3}He,t)^{48}V measurements, the observed GT strength was mainly concentrated in the E_x region below 6 MeV [13,14]. On the other hand, in the measurements on ^{56}Fe and ^{60}Ni nuclei, the main part of the GT strength was found in the higher E_x region. It is suggested that such evolution of the GT strength distribution as a function of mass number A can be explained by the competition of the active isoscalar (IS) and isovector (IV) residual interactions [18]. In this report we extend the study to the largest mass $T_z = +2$ nucleus ^{64}Zn.

II. EXPERIMENT

The ^{64}Zn(^{3}He,t)^{64}Ga experiment was performed at the high resolution facility of the Research Center for Nuclear Physics (RCNP) [19] in Osaka, Japan. The facility operates a K400 ring cyclotron [19], the WS beamline [20] designed for the realization of lateral and angular dispersion matchings, and the two quadrupole and two dipole magnets type Grand Raiden spectrometer [21]. The ^{3}He^{2+} beam was preaccelerated by a $K = 120$ MeV cyclotron and boosted to a beam energy of $E_b = 140$ MeV/nucleon by the K400 ring cyclotron. The energy spread of the beam was $\Delta E_b \approx 120$ keV. In order to achieve an experimental energy resolution better than the energy spread of the beam, *lateral dispersion matching* and *focus matching* were applied to the WS beamline and the Grand Raiden spectrometer [22]. The matching conditions were achieved by applying the faint beam method, a diagnostic procedure for the matching and focusing conditions [6].

During the experiment, the 40 e nA ^{3}He beam was transported to a ^{64}Zn target with an enrichment of 98–99% (see the discussion in Sec. III A). To maintain the good energy resolution we used a thin (1.09 mg/cm^2) self-supporting foil. The incoming ^{3}He particles have an atomic charge 2^+ while the outgoing tritons have 1^+. Therefore, the total energy loss is different depending on the travel distance of the ^{3}He particle through the target before making the (^{3}He,t) reaction. This effect caused an additional energy straggling, which largely contributed to the achieved energy resolution of 34 keV. Scattering experiments performed at 0° can suffer from a large background. In (^{3}He,t) experiments, however, the incident ^{3}He particles are in a 2+ charged state and thus have a magnetic rigidity $B\rho$ of about half of the tritons. As a result, the ^{3}He^{2+} beam was stopped in a Faraday cup inside the first dipole magnet of the Grand Raiden spectrometer.

The outgoing tritons from the target were momentum analyzed by the Grand Raiden spectrometer within its full acceptance. A system consisting of two multiwire drift chambers and two scintillators was used for the detection of particle rays at the focal plane position. The detection efficiency was constant over the full focal plane. In order to achieve a good resolution in the scattering angle $\Theta = \sqrt{\theta^2 + \phi^2}$, *angular dispersion matching* [22] was applied and Grand Raiden was operated in the *overfocus mode* [7]. This way, we achieved an angular resolution of $\Delta\Theta = 2.1$ mr. For the calibration of the scattering angle at the target position, a multihole slit was placed downstream from the target in a ^{70}Zn(^{3}He,t)^{70}Ga calibration run. The Q value of the ^{70}Zn(^{3}He,t)^{70}Ga reaction is smaller ($Q = -0.654(2)$ MeV [23]) than the Q value of the ^{64}Zn(^{3}He,t)^{64}Ga reaction ($-7.171(2)$ MeV [24]) and therefore states in ^{70}Ga were observed in a wider range of the focal plane detectors.

III. DATA ANALYSIS

A. Excitation energy

As is shown in Table I, only a few 1^+ states are known in ^{64}Ga [24]. These states have E_x values less than 1 MeV. For the energy calibration of observed states up to higher excitation energies, we used a spectrum measured with a thin

TABLE I. States observed in the region of $E_x = 0.0$–4.0 MeV. Columns 1 and 2 show the evaluated E_x and J^π values of states [24] that were also identified in our analysis. In columns 3–6, we list all states that were observed in our analysis. Each state is listed with its E_x value, momentum transfer ΔL, the counts of the respective peak in the "0° cut" spectrum, and the B(GT) value for states with $\Delta L = 0$ or $\Delta L = (0)$.

Evaluated values [24]		^{64}Zn(^{3}He,t)^{64}Ga[a]			
E_x (MeV)	J^π	E_x (MeV)	ΔL	Counts (0°)	B(GT)
0.12805 (10)	(1^+)	0.127	0	1291 (36)	0.034 (2)
0.42703 (6)	(1^+)	0.426	0	5755 (76)	0.152 (7)
0.55029 (11)	$(1,2^+)$	0.547	$\geqslant 1$	154 (13)	
0.66694 (16)	(1^+)	0.666	0	3199 (57)	0.084 (4)
0.8174 (3)	(1^+)	0.818	(0)	1263 (36)	0.033 (2)
0.937 (2)	$(1^+, 0^+)$	0.941	0	1752 (42)	0.046 (2)
		1.030	$\geqslant 1$	317 (18)	
		1.065	(0)	96 (12)	$\geqslant 0.01$
		1.235	$\geqslant 1$	127 (12)	
		1.268	$\geqslant 1$	66 (9)	
		1.365	$\geqslant 1$	59 (9)	
		1.430	$\geqslant 1$	893 (30)	
		1.540	$\geqslant 1$	68 (9)	
		1.685	$\geqslant 1$	574 (24)	
		1.759	$\geqslant 1$	246 (16)	
		1.803	0	5560 (75)	0.148 (7)
		1.864	$\geqslant 1$	5489 (74)	
1.9051(23)	(0^+)	1.923	0	16499 (129)	
		1.991	$\geqslant 1$	261 (16)	
		2.189	$\geqslant 1$	1177 (35)	
		2.223	$\geqslant 1$	127 (12)	
		2.313	$\geqslant 1$	312 (18)	
		2.356	$\geqslant 1$	53 (8)	
		2.448	$\geqslant 1$	1901 (44)	
		2.585	0	938 (31)	0.025 (1)
		2.645	0	599 (25)	0.016 (1)
		2.730	$\geqslant 1$	1433 (38)	
		2.874	$\geqslant 1$	169 (14)	
		2.913	0	957 (32)	0.026 (1)
		2.994	$\geqslant 1$	268 (18)	
		3.084	0	409 (21)	0.011 (1)
		3.168	$\geqslant 1$	62 (8)	
		3.222	0	8120 (90)	0.219 (10)
		3.289	0	3031 (55)	0.082 (4)
		3.332	0	2228 (47)	0.060 (3)
		3.430	$\geqslant 1$	1405 (38)	
		3.527	0	3165 (56)	0.086 (4)
		3.586	$\geqslant 1$	601 (25)	
		3.690	$\geqslant 1$	351 (19)	
		3.764	$\geqslant 1$	930 (35)	
		3.829	0	1513 (40)	0.041 (2)
		3.911	0	784 (28)	0.021 (1)
		3.954	$\geqslant 1$	668 (26)	

[a]Present work.

(1.03 mg/cm^2) natural magnesium target (^{nat}Mg: 79.0% ^{24}Mg, 10.0% ^{25}Mg, 11.0% ^{26}Mg). Several (^{3}He,t) reaction runs on the ^{nat}Mg target were performed under the same conditions as the ^{64}Zn runs. The Q values of the (^{3}He,t) reaction on ^{24}Mg, ^{25}Mg and ^{26}Mg are $-13.886(1)$ MeV [25], $-4.276(1)$ MeV [26] and $-4.004(1)$ MeV [27], respectively. Owing to the different Q values, states of the final nuclei ^{24}Al, ^{25}Al, and ^{26}Al are positioned across a wide range of the focal plane detectors. Owing to the large Q value of the ^{64}Zn(^{3}He,t)^{64}Ga reaction, the position of ^{64}Ga states up to ≈11 MeV lie inside the region covered by the known aluminum states. The E_x values of the known ^{64}Ga and the Al states were used to calculate the $B\rho$ values at the positions of these states in the focal plane using kinematic calculations. As a result, the positions in the focal plane could be correlated to $B\rho$ values. The difference in target thickness of the ^{64}Zn

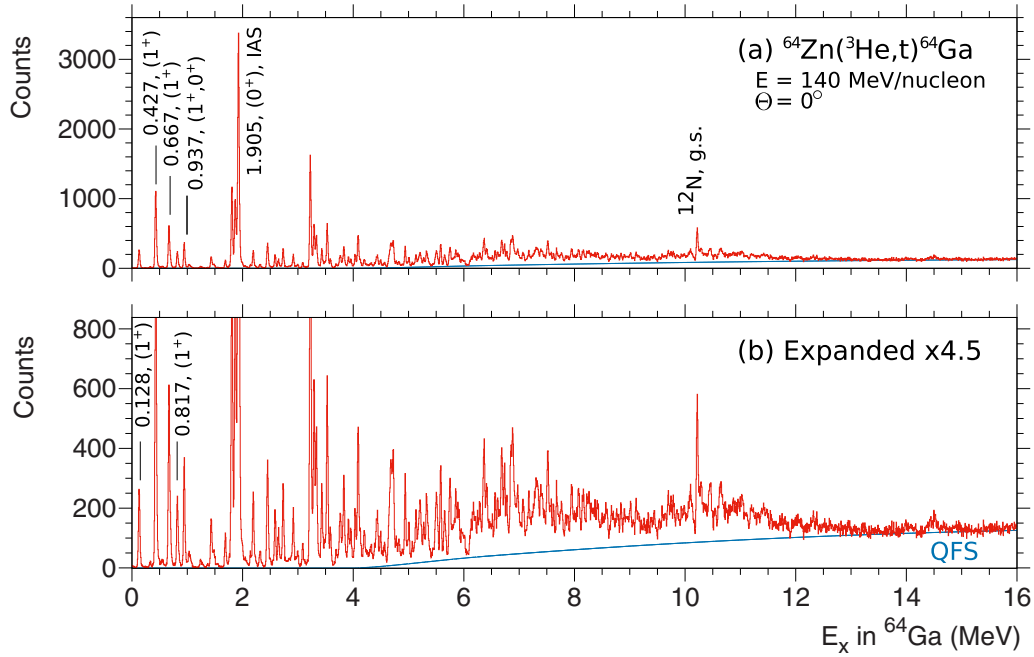

FIG. 2. Triton spectrum of the ^{64}Zn(^{3}He,t)^{64}Ga reaction at 0° on two scales given as a function of the excitation energy (E_x) of states in the final nucleus ^{64}Ga. Prominent peaks which were identified with literature partners are labeled with their E_x values. The literature J^π values are given. The expected contribution of the quasifree scattering (QFS) to the spectrum is indicated by a solid line. The counts below the QFS line were subtracted in the data analysis.

and the $^{\text{nat}}$Mg target causes a difference in the total energy loss inside the target. This effect was taken into account in the calibration process. The excitation energies of the known ^{64}Ga states were reproduced with less than 4 keV deviation (see Table I). The energy-calibrated spectrum is shown in Fig. 2.

The most prominent peak in the spectrum at $E_x = 1.923$ MeV is the isobaric analog state (IAS) which is the analog state of the g.s. of the initial ^{64}Zn nucleus. Because of the similar structure of the g.s. of the initial nucleus and the IAS, the IAS often dominates the spectrum in β decays and CE reactions [2]. As a result, its excitation energies are usually well studied. However, our E_x value of the IAS state deviates by 18 keV from the adopted literature value of $E_x = 1.9051(23)$ MeV [24].

The energy displacement of the IAS can be caused by target contamination from target material isotopes. The IASs in (^{3}He,t) reactions performed on different isotopes have similar Q values. Therefore, if the isotopic contamination of the target material is large, the IASs of the contaminants can shift the center position of the IAS in the ^{64}Ga spectrum. The contributions of other isotopes were examined by comparing with the ^{66}Ga, ^{68}Ga, and ^{70}Ga spectra that were taken under the same conditions as the ^{64}Ga spectrum. Note that the reaction Q values, i.e., g.s.-g.s. Q values, decrease with the increase of mass number A. They are -7.171 MeV [24] for $A = 64$, $-5.175(3)$ MeV [28] for $A = 66$, $-2.921(1)$ MeV [29] for $A = 68$, and $-0.654(2)$ MeV [23] for $A = 70$. Therefore, the low-lying states of ^{66}Ga, ^{68}Ga, and ^{70}Ga can appear in the energy region below the ^{64}Ga g.s. As a result of the comparison, we identified a few ^{66}Ga states in the ^{64}Ga spectrum. It is worth pointing out that no ^{68}Ga and ^{70}Ga states were observed. None of the observed ^{66}Ga states have heights of more than 20 counts. In the reference ^{66}Ga spectrum, the IAS is approximately two times higher than the ^{66}Ga states that we found in the ^{64}Ga spectrum. Therefore, the ^{66}Ga IAS can contribute at most 40 counts to the heights of the IAS in the ^{64}Ga spectrum. Because the IAS in the ^{64}Ga spectrum has a height of about 3400 counts (see Fig. 2) we estimate the isotopic enrichment of the ^{64}Zn target to be 98–99%. Therefore, the isotopic contamination of the target can not cause the 18 keV displacement of the IAS.

We could also identify states from ^{12}C and ^{16}O contaminants in our ^{64}Ga spectrum. The (^{3}He,t) reaction performed on ^{16}O has a Q value of $Q = -15.417(9)$ MeV [30]. Therefore, we expect excited states of the final nucleus ^{16}F above 8.3 MeV in the ^{64}Ga spectrum. Previous (^{3}He,t) experiments performed under similar conditions show that the most prominent state contributing to the spectrum is the $J^\pi = 2^-$ state at 0.424(5) MeV [31]. We identified the 0.424 MeV state in ^{16}F at 8.740 MeV in the ^{64}Ga spectrum on the basis of its different kinematic behavior. Because this state was only weakly excited in the ^{64}Ga spectrum, we estimate that the contribution of other ^{16}F states to the ^{64}Ga spectrum is also small. The Q value of the (^{3}He,t) reaction on ^{12}C is $Q = -17.338(1)$ MeV [32]. We observed the ^{12}N g.s. at 10.22 MeV in the ^{64}Ga spectrum (see Fig. 2). We used this state to estimate the accuracy of the energy calibration in this high excitation energy region. The E_x value of the ^{12}N g.s. was reproduced with a 5 keV deviation.

As mentioned above, we were able to reproduce the E_x values of all known states in the ^{64}Ga spectrum within 4 keV

deviation. In addition, we reproduced the E_x value of ^{12}N g.s. at 10.22 MeV with 5 keV difference. We therefore estimate that the deviation of E_x values for states below 10.22 MeV is about 5 keV, at least for the states with good statistics. Furthermore, we could exclude the contribution to the IAS caused by isotopic contaminants of the target. For that reason, we think that our E_x value of 1.923 MeV, as determined in our analysis, is preferred over the literature value $E_x =$ 1.9051(23) MeV.

B. Quasifree scattering

As shown in Fig. 2, above the proton separation energy $S_p = 3.909(2)$ MeV, it is expected that the proton knockout reaction with a three-body kinematics makes a continuous structure in the spectrum. This so-called *quasifree scattering* (QFS) can be described by an empirical function introduced in Ref. [33]. We produced spectra with angle cuts of (0) 0.0°–0.5°, (1) 0.5°–0.8°, (2) 0.8°–1.2°, (3) 1.2°–1.6°, and (4) 1.6°–2.0° labeled as Θ_j. The continuum caused by the QFS process in the present $\Theta_{j=0}$ spectrum (0.0°–0.5°) was estimated following the formalism described in Ref. [33]. We assume that the $E_x \gtrsim 13$ MeV region of the spectrum, where almost no prominent peak appears, mostly consists of the QFS so that the parameters were optimized to reproduce this region [see Fig. 2(b)].

C. Assignment of angular momentum transfer ΔL

Owing to the $\Delta L = 0$ nature of the GT transitions, it is expected that the angular distributions of the cross section of the GT states are forward peaked and have the largest cross sections at 0° (see Fig. 3). On the other hand, the cross sections for $\Delta L \geqslant 1$ transitions increase with the scattering angle. Therefore, we can identify the GT candidate by analyzing the angular distribution of the cross section. From now on, we refer to the 0.0°–0.5° cut as the "0° cut" and the others as the "finite-angle cuts".

We determined the ratio of the cross sections $R(\Theta_j) = \sigma(\Theta_j)/\sigma(0°)$ for the *known* 1^+ states that showed an angular distribution consistent with the IAS's [24]. The IAS is excited by the $0^+ \rightarrow 0^+$ Fermi transition and therefore 1^+ states that have a similar angular distribution should also be populated by $\Delta L = 0$ transitions. We determine the average of their $R(\Theta_j)$ values, $\hat{R}(\Theta_j)$, at each finite angle cut, i.e., $j = 1$, 2, 3, and 4. Similarly we determine the ratio of cross sections for *all* observed states. These ratios are then normalized by their respective $\hat{R}(\Theta_j)$ value:

$$r(\Theta_j) = \frac{\sigma(\Theta_j)}{\sigma(0°)} \Big/ \hat{R}(\Theta_j), \quad j = 1, 2, 3, 4. \tag{3}$$

We suggest that all states showing a normalized ratio of $r(\Theta_j) \approx 1$ for $j = 1$, 2, 3, and 4 should be attributed to $\Delta L = 0$ states, while those showing an $r(\Theta_j) \neq 1$ have $\Delta L \geqslant 1$ character. Note that the cross section of the GT transition to the 1^+ state is the largest in the $\sigma(0°)$ cut and decreases at larger angle cuts.

At $E_b = 140$ MeV/nucleon and scattering angles close to 0°, the ratio of the cross sections $\sigma(\Theta)/\sigma(0°)$ for each state is approximately proportional to the ratio of the yield $y(\Theta)/y(0°)$ of the respective peak in the spectrum. Therefore, the $r(\Theta_j)$ values can be determined by comparing the peak yields in the finite angle cuts to the peak yield in the 0° cut. We extracted the yield of all states up to $E_x = 5.9$ MeV in all angular cuts by using the computer program S-FIT [34] for peak deconvolution. Above 5.9 MeV, the level density is high, and for that reason only prominent peaks could be reliably analyzed. Above 10.7 MeV, the level density was too high to separate individual peaks.

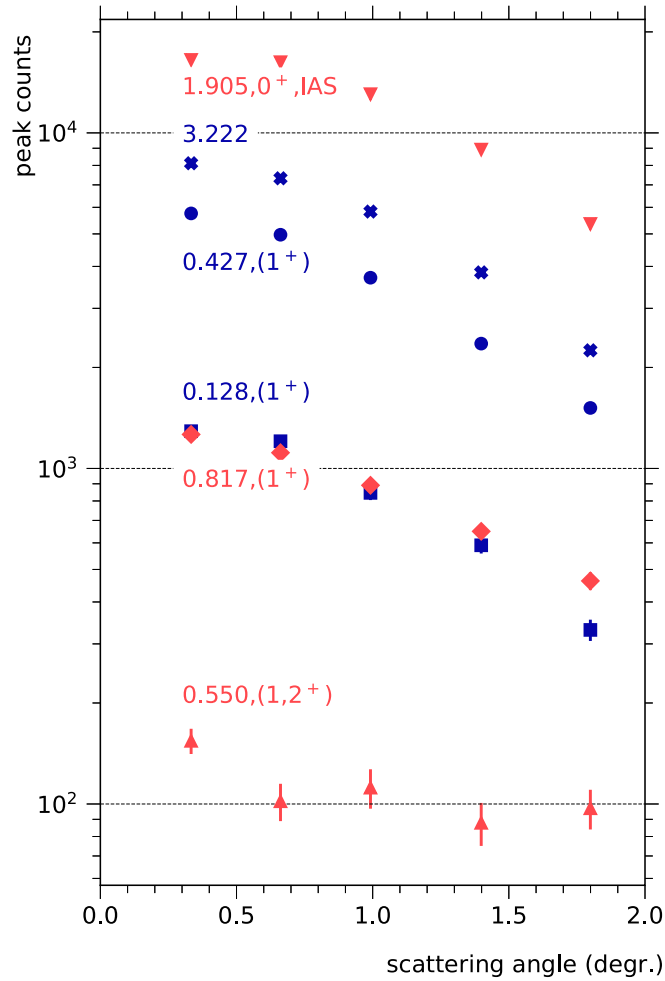

FIG. 3. Angular distribution of $\Delta L = 0$ and $\Delta L \geqslant 1$ states in the low E_x region of the present (^{3}He,t) measurement. The vertical axis shows the counts of states in the respective angular cut spectrum (see Table I). The counts for the states in the finite-angle cuts are corrected by the ratios of the solid angles. States that were identified as GT candidates in our analysis are shown by the blue markers. Other states are indicated by red markers. Literature E_x and J^π values are presented [24].

The $r(\Theta_j)$ values for all states separated in the deconvolution process are shown in Fig. 4. States which exhibit $r(\Theta_j)$ ratios deviating no more than 25% from unity were selected as $\Delta L = 0$. When the error bars were inside 25% deviation, they were also accepted as $\Delta L = 0$ candidates although their $\Delta L = 0$ assignments are less certain. Therefore, we indicate these states in our tables by the label "(0)". States with $r(\Theta_j)$

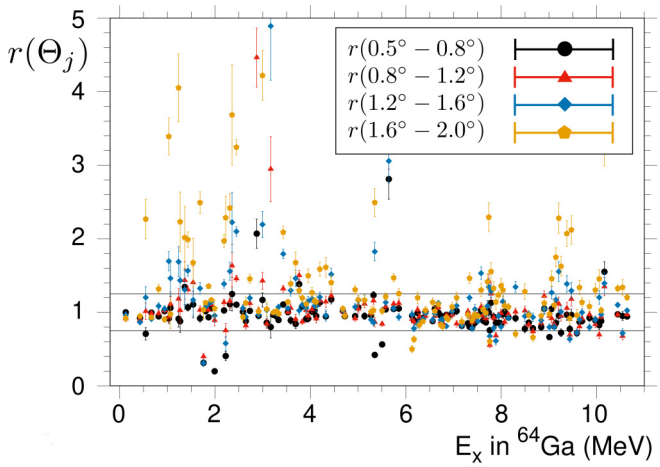

FIG. 4. Normalized ratios $r(\Theta_j)$ of all separated states in the spectrum. The horizontal lines indicate 25% deviation from unity. States with all ratios close to unity are selected as GT candidates.

values that deviated more than 25% from unity were assigned to have $\Delta L \geqslant 1$. States that showed large ambiguities in the peak deconvolution process were not included in the analysis. The results of the ΔL assignment are shown in Tables I–IV. It should be noted that the main part of the observed strengths show consistent $r(\Theta)$ values as $\Delta L = 0$ or (0) regardless of the existence and nonexistence of the QFS. This fact strongly suggests the validity of the QFS estimation.

TABLE II. States observed in the region of $E_x = 4.0$–6.0 MeV. Each state is listed with its E_x value, momentum transfer ΔL, the counts of the respective peak in the "0° cut" spectrum, and the B(GT) value for states with $\Delta L = 0$ or $\Delta L = (0)$.

^{64}Zn(^{3}He,t)^{64}Ga[a]			
E_x (MeV)	ΔL	Counts (0°)	B(GT)
4.033	(0)	1011 (32)	0.028 (2)
4.086	0	2338 (49)	0.064 (3)
4.121	0	462 (22)	0.013 (1)
4.197	$\geqslant$1	684 (27)	
4.323	$\geqslant$1	404 (21)	
4.437	$\geqslant$1	712 (29)	
4.679	0	2570 (51)	0.071 (3)
4.721	0	1742 (42)	0.048 (2)
4.937	(0)	1343 (37)	0.037 (2)
5.004	0	688 (27)	0.019 (1)
5.134	0	831 (29)	0.023 (1)
5.272	0	681 (27)	0.019 (1)
5.322	0	1108 (34)	0.031 (2)
5.349	$\geqslant$1	433 (23)	
5.503	$\geqslant$1	1512 (41)	
5.578	0	1602 (40)	0.045 (2)
5.643	$\geqslant$1	282 (26)	
5.746	$\geqslant$1	1824 (43)	
5.853	(0)	1071 (33)	0.030 (2)

[a]Present work.

TABLE III. States clearly observed in the region of $E_x = 6.0$–9.0 MeV. Each state is listed with its E_x value, momentum transfer ΔL, the counts of the respective peak in the "0° cut" spectrum, and the B(GT) value for the states with $\Delta L = 0$ or $\Delta L = (0)$.

^{64}Zn(^{3}He,t)^{64}Ga[a]			
E_x (MeV)	ΔL	Counts (0°)	B(GT)
6.131	$\geqslant$1	620 (25)	
6.171	$\geqslant$1	897 (30)	
6.247	0	674 (27)	0.019 (1)
6.285	0	868 (30)	0.024 (1)
6.359	0	2534 (51)	0.071 (3)
6.412	0	1389 (38)	0.039 (2)
6.562	0	1256 (36)	0.035 (2)
6.608	0	830 (29)	0.023 (1)
6.682	0	2516 (51)	0.071 (3)
6.733	0	1273 (36)	0.036 (2)
6.774	0	984 (32)	0.028 (2)
6.850	0	1939 (44)	0.055 (3)
6.884	0	2009 (45)	0.057 (3)
6.971	0	920 (31)	0.026 (1)
7.065	0	767 (28)	0.022 (1)
7.173	0	834 (29)	0.024 (1)
7.301	0	1148 (34)	0.033 (2)
7.335	$\geqslant$1	1085 (33)	
7.389	0	931 (31)	0.027 (1)
7.416	0	755 (28)	0.022 (1)
7.450	0	629 (25)	0.018 (1)
7.511	0	2532 (51)	0.073 (4)
7.578	$\geqslant$1	601 (25)	
7.619	0	724 (27)	0.021 (1)
7.679	0	1020 (32)	0.029 (2)
7.713	$\geqslant$1	461 (22)	
7.740	$\geqslant$1	288 (17)	
7.760	$\geqslant$1	660 (26)	
7.787	$\geqslant$1	409 (20)	
7.841	(0)	612 (25)	0.018 (1)
7.888	$\geqslant$1	420 (21)	
7.942	0	1377 (38)	0.040 (2)
7.996	$\geqslant$1	517 (23)	
8.037	(0)	541 (24)	0.016 (1)
8.070	0	792 (29)	0.023 (1)
8.151	0	1883 (44)	0.055 (3)
8.300	$\geqslant$1	694 (27)	
8.496	(0)	437 (22)	0.013 (1)
8.577	0	1229 (35)	0.036 (2)
8.665	$\geqslant$1	647 (26)	
8.838	0	766 (28)	0.023 (1)
8.902	0	502 (24)	0.015 (1)

[a]Present work.

Similarly to the transitions to the 1^+ states, the angular distribution of the transitions to the 3^+ states decreases in the range from 0°–1.6° [13] (see Fig. 3). Therefore, 3^+ states exhibit $r(\Theta_j)$ values close to 1 for $\Theta < 1.6°$. However, above $\Theta = 1.6°$ the transitions to the 1^+ states have smaller $r(1.6°$–$2.0°)$ values than the transitions to 3^+ states. Therefore, 3^+ states could be distinguished by their larger $r(1.6°$–$2.0°)$ values. The prominent peak at 0.818 MeV has an

TABLE IV. States clearly observed in the region of E_x = 9.0–10.7 MeV. Each state is listed with its E_x value, momentum transfer ΔL, the counts of the respective peak in the "0° cut" spectrum, and the B(GT) value for the states with $\Delta L = 0$ or $\Delta L = (0)$.

^{64}Zn(^{3}He,t)^{64}Ga[a]			
E_x (MeV)	ΔL	Counts (0°)	B(GT)
9.010	(0)	793 (28)	0.023 (1)
9.058	$\geqslant$1	460 (22)	
9.112	0	766 (28)	0.023 (1)
9.146	$\geqslant$1	446 (21)	
9.207	$\geqslant$1	253 (16)	
9.254	$\geqslant$1	370 (20)	
9.376	$\geqslant$1	306 (18)	
9.437	$\geqslant$1	537 (23)	
9.471	$\geqslant$1	260 (16)	
9.586	(0)	536 (23)	0.016 (1)
9.641	(0)	540 (23)	0.016 (1)
9.695	0	989 (32)	0.030 (2)
9.851	0	707 (27)	0.021 (1)
9.973	(0)	671 (26)	0.020 (1)
10.055	$\geqslant$1	352 (19)	
10.095	0	1798 (43)	0.054 (3)
10.163	$\geqslant$1	192 (14)	
10.442	(0)	2737 (53)	0.083 (4)
10.544	(0)	428 (21)	0.013 (1)
10.639	(0)	2789 (53)	0.085 (4)

[a]Present work.

angular distribution similar to a 3^+ state. The evaluated J^π of this state is $J^\pi = 1^+$; therefore, we label this state as $(1^+, 3^+)$. Furthermore, the angular distribution of a state at 0.550 MeV is also shown in Fig. 3. The literature J^π value of this state is $(1, 2^+)$. Because its angular distribution is clearly different from the IAS and other 1^+ states, this state was not selected as a GT candidate.

D. Gamow-Teller transition strength

We observed discrete states up to 10.7 MeV in the ^{64}Zn(^{3}He,t)^{64}Ga reaction. The B(GT) values of these states were deduced by using the proportionality given by Eq. (2). We calculated the energy dependence of $F(q, \omega)$ by DWBA caluclations, using the DWBA code DW81 [35] and following the procedure described in [36–38]. We assumed that the transition are mostly of $\nu f_{7/2} \rightarrow \pi f_{5/2}$ configuration. The optical potential parameters were taken from [39]. The DWBA calculations show that $F(q, \omega)$ decreases with increasing excitation energy. At 10.7 MeV $F(q, \omega)$ decreases to 85% of the value for the ^{64}Ga g.s. In order to determine absolute B(GT) values we used the R^2 value defined as in [3]:

$$R^2 = \frac{\hat{\sigma}_{GT}}{\hat{\sigma}_F} \quad (4)$$

$$= \frac{\sigma_{GT}(0^\circ)}{B(GT)} \frac{B(F)}{\sigma_F(0^\circ)}, \quad (5)$$

where $\hat{\sigma}_{GT}$ and $\hat{\sigma}_F$ are the GT and the Fermi (F) unit cross sections and $\sigma_{GT}(0^\circ)$ and $\sigma_F(0^\circ)$ are the DWBA corrected GT and F cross sections at $q = \omega = 0$ with $\sigma_{GT}(0^\circ) = \hat{\sigma}_{GT} B(GT)$ and $\sigma_F(0^\circ) = \hat{\sigma}_F B(F)$. We assume that the full Fermi strength $B(F) = |N - Z| = 4$ is concentrated in the IAS, with $\sigma_F(0^\circ)$ proportional to the yield of the IAS. On the other hand, the values of $\sigma_{GT}(0^\circ)$ are proportional to the yield of the peaks for the respective transitions in the spectrum. R^2 values have been determined for various mass A nuclei throughout the nuclear chart by combining (^{3}He,t) and β decay experiments [40,41]. We determined the R^2 for ^{64}Zn by fitting the mass A dependence of the known R^2 values assuming a smooth function, and interpolated the result to ^{64}Zn. The R^2 value of ^{64}Zn was determined to be $R^2 = 9.1(4)$. We determined the B(GT) values for all GT candidates using Eq. (2), taking into account the uncertainties of the peak yields and the R^2 value. The resulting B(GT) values for all GT transitions are summarized in Tables I–IV.

IV. RESULTS AND DISCUSSION

A. B(GT) distibution in ^{64}Ga

Below $E_x = 5.9$ MeV, the GT strength is rather concentrated into a few strong states (see Fig. 5). In this region, the low level density allowed a clear separation in the peak deconvolution process resulting in a precise determination of GT candidates and their transition strengths (see Tables I and II). On the other hand, owing to the increasing level density, only prominent peaks could be analyzed in the peak deconvolution process in the region between 6.0 and 10.7 MeV. Thus, the GT strength presented in Tables III and IV is the minimum of the real GT strength in this region. Above 10.7 MeV, where the level density is even higher, states could not be separated by peak deconvolution.

We compared our results with shell-model calculations [10,12] performed using the GXPF1J interaction. In these calculations, transitions can be classified by the isospin T value of the final state in ^{64}Ga. The results of the calculations are shown in Fig. 5(b). In the region below 10 MeV, the GT strength distribution is dominated by the transitions to the $T = T_0 - 1 = 1$ states. These states are constructed on top of the g.s. of ^{64}Ga and are therefore expected at low excitation energies (see Fig. 1). On the other hand, the $T = T_0 = 2$ states are constructed on top of the g.s. of ^{64}Zn. Thus, these states are expected at excitation energies above the E_x value of the IAS which is $E_x = 1.923$ MeV. However, the SM calculations suggest that only a minor part of the GT strength in the region below 10 MeV can be attributed to the transitions to the $T = 2$ states. According to the calculations, the main part of the $T = 2$ strength is concentrated in a wide resonance-like structure around 12 MeV. In addition, the SM calculations predict weakly excited $T = 3$ states between 14 and 16 MeV. The $T = 3$ states are constructed on top of the g.s. of ^{64}Cu and are, therefore, located at these high excitation energies.

B. Total B(GT) strength

Figure 6 shows the experimental and SM cumulative sums (CS) of the GT strength below 10.7 MeV, where level-by-level analysis was performed. Up to $\approx$ 7 MeV the experimental CS is well reproduced by the SM calculations. As noted before,

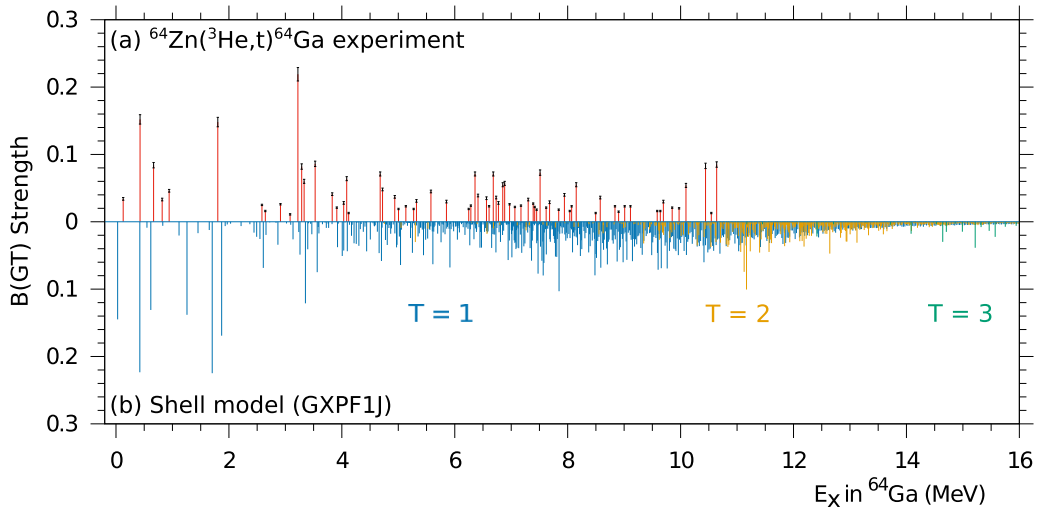

FIG. 5. Gamow-Teller strength distribution determined from the (a) ^{64}Zn(^{3}He,t)^{64}Ga experiment and (b) shell-model calculations. Above 10.7 MeV, the level density was too high to separate all individual states. The SM calculations used the GXPF1J interaction. Here, we did not include a quenching factor.

above 6 MeV, we could not analyze all states owing to the high level-density (see Tables III and IV). In this region, the SM CS exceed the experimental CS. The experimental CS value up to 10.7 MeV is 2.89(2) compared to a SM CS value of 6.05 at this energy.

C. Comparison with the ^{64}Zn(d, ^{2}He)^{64}Cu experiment

Under the assumption of isospin being a good quantum number, the GT$_-$ and GT$_+$ type transitions connecting the g.s. of ^{64}Zn with the $T = 3$ states in the final nuclei ^{64}Ga and ^{64}Cu should exhibit similar relative strengths and excite a similar structure of states. As described above, the GT$_+$ transitions starting from ^{64}Zn were studied in a ^{64}Zn(d, ^{2}He)^{64}Cu experiment [42]. The resolution in the (d, ^{2}He) experiment was of the order of ≈115 keV. Because ^{64}Cu has $T_z = +3$, only states with isospin $T = 3$ were excited by the GT$_+$ transitions (see Fig. 1). These states are analogous to the $T = 3$ states in ^{64}Ga. Therefore, we expect corresponding excitation energies and transition strengths for these states in ^{64}Ga and ^{64}Cu. As is shown in Fig. 5, the SM calculations suggest that the main part of the GT$_-$ strength going to the $T = 3$ states is concentrated around 11–16 MeV. It is expected that these transitions are relatively weak due to the small Clebsch-Gordon coefficient of $C^2_{\rm GT} = 1/15$, as shown in Fig 1. We compared the features of this region in the ^{64}Ga spectrum with those in the ^{64}Cu spectrum and found a good correspondence for some states (see Fig. 7). Especially the pronounced peaks in the ^{64}Cu spectrum at 2.66 and 3.19 MeV are in good agreement with peaks found in our ^{64}Ga spectrum. These states have E_x values of 13.99 and 14.51 MeV in ^{64}Ga and the relative height of these states is similar in both spectra. For the state at 2.78 MeV, we found a corresponding candidate at 14.08 MeV. We note that this state was not observed in recent ^{64}Ni (^{3}He,t)^{64}Cu data [43], and therefore the $T = 3$ identification of this state is less certain. For the ^{64}Cu states at 0 MeV (g.s.), 0.2–0.6 MeV, 0.95 MeV, and 1.52 MeV we could not reliably find corresponding partners in ^{64}Ga owing to the high level density and the weakness of the transitions to these states. In the 4–5 MeV region, the strength is spread across a few weak transitions. Again, we could not identify corresponding partners in the ^{64}Ga spectrum. In conclusion, we suggest a tentative isospin $T = 3$ assignment for the ^{64}Ga states at 13.99 and 14.51 MeV. We note that we increased the channel width of our ^{64}Zn(^{3}He,t)^{64}Ga data in Fig. 7(a). This decreased the energy resolution of the spectrum in Fig. 7 to 50 keV but made the data more accessible for analysis. The given ^{64}Ga excitation energies were determined from the center of the corresponding structure.

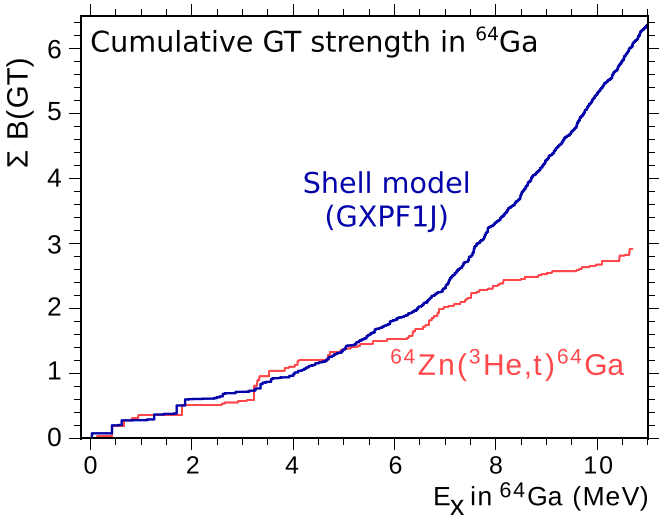

FIG. 6. Comparison of the cumulative Gamow-Teller strength distribution from the ^{64}Zn(^{3}He,t)^{64}Ga experiment (red line) and the shell-model calculations (blue line) below 10.7 MeV. A quenching factor of $(0.74)^2$ is included in the SM result. The thickness of the experimental line (red) represents the error of the sum at any given point.

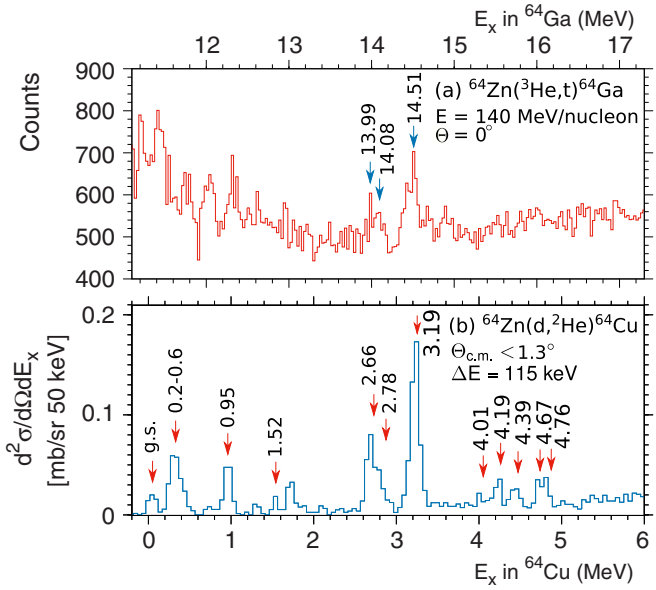

FIG. 7. Comparison of the (a) ^{64}Zn(^{3}He,t)^{64}Ga and (b) ^{64}Zn(d, ^{2}He)^{64}Cu spectra [42]. Corresponding states are labeled with their respective excitation energy. We suggest that the pronounced states at 13.99 and 14.51 MeV are of isospin $T = 3$ nature and have $J^\pi = 1^+$. The channel width in (a) was increased compared to the spectrum shown in Fig. 2 to even out statistical fluctuations.

V. SUMMARY

We measured GT transitions starting from ^{64}Zn to ^{64}Ga using a CE-type (^{3}He,t) reaction at RCNP, Osaka. The measurements were performed at 0° and 140 MeV/nucleon. The achieved energy resolution was 34 keV. Candidates of GT states were identified by their characteristic $\Delta L = 0$ angular distribution obtained for the angle range of 0°–2°. We derived the GT transitions strength for all GT candidates. We could analyze all states below 6 MeV in the spectrum. In this region, the GT strength distribution is rather fragmented. As a result of the increasing level density, only strong states could be analyzed above 6 MeV. Above 10.7 MeV the level density was too high to separate individual states with a few exceptions around 14 MeV. We compared the cumulative sum of the GT strength with the SM calculations. The SM calculations showed good agreement with our data in the region below 6 MeV. At higher energies the SM calculations did not reproduce the measured GT strength. The SM calculations also suggest that the GT strength below 10 MeV can mostly be attributed to transitions to the $T = 1$ states while the $T = 2$ states are concentrated around 12 MeV and the $T = 3$ states around 15 MeV. We compared our data with the results of a ^{64}Zn(d, ^{2}He)^{64}Cu experiment and were able to identify prominent transitions around 14 MeV with probable $T = 3$ character, showing the robustness of the isospin quantum number up to $T_z = +3$.

ACKNOWLEDGMENTS

The (^{3}He,t) experiments were performed at RCNP, Osaka University under the Experimental Program E378. The authors thank the accelerator group of RCNP for providing a high-quality ^{3}He beam. F.C., E.G., and B.R. thank RCNP, Osaka University, Japan for the support of their stay in Osaka. This work was partly supported by the RIKEN-CNS joint research project on large-scale nuclear-structure calculations. The authors thank Prof. D. Frekers for providing the ^{64}Zn(d, ^{2}He)^{64}Cu spectrum. F.D. wishes to thank Prof. P. v. Brentano for valuable discussions. F.D. and J.J. acknowledge the support by the DFG (Grant No. J0 391/17-1). Y.F., H.F., and A.T. acknowledge the support by JSPS KAKENSHI, Japan under Grants No. 15540274, No. 18540270, and No. JP15K05104. Y.F. and B.R. acknowledge the support of the Japan-Spain collaboration program by JSPS and CSIC. B.R. acknowledges the support of Spanish Ministry (Grant No. FPA2014-52823-C2-1-P and Centro de Excelencia Severo Ochoa del IFIC SEV-2014-0398). This work was supported by the Bonn-Cologne Graduate School for Physics and Astronomy (BCGS), the FrontierLab@OsakaU program, and the Japanese Student Service Organization (JASSO).

[1] F. Osterfeld, Rev. Mod. Phys. **64**, 491 (1992).
[2] Y. Fujita, B. Rubio, and W. Gelletly, Prog. Part. Nucl. Phys. **66**, 549 (2011).
[3] T. Taddeucci, C. Goulding, T. Carey, R. Byrd, C. Goodman, C. Gaarde, J. Larsen, D. Horen, J. Rapaport, and E. Sugarbaker, Nucl. Phys. A **469**, 125 (1987).
[4] W. G. Love, K. Nakayama, and M. A. Franey, Phys. Rev. Lett. **59**, 1401 (1987).
[5] J. Rapaport and E. Sugarbaker, Annu. Rev. Nucl. Part. Sci. **44**, 109 (1994).
[6] H. Fujita, Y. Fujita, G. Berg, A. Bacher, C. Foster, K. Hara, K. Hatanaka, T. Kawabata, T. Noro, H. Sakaguchi, Y. Shimbara, T. Shinada, E. Stephenson, H. Ueno, and M. Yosoi, Nucl. Instrum. Methods A **484**, 17 (2002).
[7] H. Fujita, G. Berg, Y. Fujita, K. Hatanaka, T. Noro, E. Stephenson, C. Foster, H. Sakaguchi, M. Itoh, T. Taki, K. Tamura, and H. Ueno, Nucl. Instr. Meth. A **469**, 55 (2001).
[8] K. Langanke and G. Martínez-Pinedo, Rev. Mod. Phys. **75**, 819 (2003).
[9] T. Otsuka, M. Honma, T. Mizusaki, N. Shimizu, and Y. Utsuno, Prog. Part. Nucl. Phys. **47**, 319 (2001).
[10] M. Honma, T. Otsuka, T. Mizusaki, M. Hjorth-Jensen, and B. Brown, J. Phys.: Conf. Ser. **20**, 7 (2005).
[11] M. Honma, T. Otsuka, B. A. Brown, and T. Mizusaki, Phys. Rev. C **65**, 061301(R) (2002).
[12] M. Honma, T. Otsuka, B. A. Brown, and T. Mizusaki, Phys. Rev. C **69**, 034335 (2004).
[13] Y. Fujita, T. Adachi, H. Fujita, A. Algora, B. Blank, M. Csatlós, J. M. Deaven, E. Estevez-Aguado, E. Ganioğlu, C. J. Guess, J. Gulyás, K. Hatanaka, K. Hirota, M. Honma, D. Ishikawa, A. Krasznahorkay, H. Matsubara, R. Meharchand, F. Molina, H. Okamura, H. J. Ong, T. Otsuka, G. Perdikakis, B. Rubio, C. Scholl, Y. Shimbara, E. J. Stephenson, G. Susoy, T. Suzuki, A. Tamii, J. H. Thies, R. G. T. Zegers, and J. Zenihiro, Phys. Rev. C **88**, 014308 (2013).

[14] E. Ganioğlu, H. Fujita, B. Rubio, Y. Fujita, T. Adachi, A. Algora, M. Csatlós, J. M. Deaven, E. Estevez-Aguado, C. J. Guess, J. Gulyás, K. Hatanaka, K. Hirota, M. Honma, D. Ishikawa, A. Krasznahorkay, H. Matsubara, R. Meharchand, F. Molina, H. Okamura, H. J. Ong, T. Otsuka, G. Perdikakis, C. Scholl, Y. Shimbara, G. Susoy, T. Suzuki, A. Tamii, J. H. Thies, R. G. T. Zegers, and J. Zenihiro, Phys. Rev. C **93**, 064326 (2016).
[15] Y. Fujita, H. Fujita, B. Rubio, W. Gelletly, and B. Blank, Acta Phys. Pol. B **43**, 153 (2012).
[16] H. Fujita, Y. Fujita, T. Adachi, H. Akimune, N. T. Botha, K. Hatanaka, H. Matsubara, K. Nakanishi, R. Neveling, A. Okamoto, Y. Sakemi, T. Shima, Y. Shimizu, F. D. Smit, T. Suzuki, A. Tamii, and M. Yosoi, Phys. Rev. C **88**, 054329 (2013).
[17] L. Popescu (private communication).
[18] Y. Fujita, H. Fujita, T. Adachi, C. L. Bai, A. Algora, G. P. A. Berg, P. von Brentano, G. Colò, M. Csatlós, J. M. Deaven, E. Estevez-Aguado, C. Fransen, D. De Frenne, K. Fujita, E. Ganioğlu, C. J. Guess, J. Gulyás, K. Hatanaka, K. Hirota, M. Honma, D. Ishikawa, E. Jacobs, A. Krasznahorkay, H. Matsubara, K. Matsuyanagi, R. Meharchand, F. Molina, K. Muto, K. Nakanishi, A. Negret, H. Okamura, H. J. Ong, T. Otsuka, N. Pietralla, G. Perdikakis, L. Popescu, B. Rubio, H. Sagawa, P. Sarriguren, C. Scholl, Y. Shimbara, Y. Shimizu, G. Susoy, T. Suzuki, Y. Tameshige, A. Tamii, J. H. Thies, M. Uchida, T. Wakasa, M. Yosoi, R. G. T. Zegers, K. O. Zell, and J. Zenihiro, Phys. Rev. Lett. **112**, 112502 (2014).
[19] See web site http://www.rcnp.osaka-u.ac.jp.
[20] T. Wakasa, K. Hatanaka, Y. Fujita, G. Berg, H. Fujimura, H. Fujita, M. Itoh, J. Kamiya, T. Kawabata, K. Nagayama, T. Noro, H. Sakaguchi, Y. Shimbara, H. Takeda, K. Tamura, H. Ueno, M. Uchida, M. Uraki, and M. Yosoi, Nucl. Instrum. Methods A **482**, 79 (2002).
[21] M. Fujiwara, H. Akimune, I. Daito, H. Fujimura, Y. Fujita, K. Hatanaka, H. Ikegami, I. Katayama, K. Nagayama, N. Matsuoka, S. Morinobu, T. Noro, M. Yoshimura, H. Sakaguchi, Y. Sakemi, A. Tamii, and M. Yosoi, Nucl. Instrum. Methods A **422**, 484 (1999).
[22] Y. Fujita, K. Hatanaka, G. Berg, K. Hosono, N. Matsuoka, S. Morinobu, T. Noro, M. Sato, K. Tamura, and H. Ueno, Nucl. Instrum. Methods Phys. Res. Sect. B **126**, 274 (1997).
[23] G. Gurdal and E. McCutchan, Nucl. Data Sheets **136**, 1 (2016).
[24] B. Singh, Nucl. Data Sheets **108**, 197 (2007).
[25] R. Firestone, Nucl. Data Sheets **108**, 2319 (2007).
[26] R. Firestone, Nucl. Data Sheets **110**, 1691 (2009).
[27] M. Basunia and A. Hurst, Nucl. Data Sheets **134**, 1 (2016).
[28] E. Browne and J. Tuli, Nucl. Data Sheets **111**, 1093 (2010).
[29] E. McCutchan, Nucl. Data Sheets **113**, 1735 (2012).
[30] J. Kelley, D. Tilley, H. Weller, and C. Cheves, Nucl. Phys. **564**, 1 (1993).
[31] Y. Fujita, H. Fujita, T. Adachi, G. Susoy, A. Algora, C. L. Bai, G. Colò, M. Csatlós, J. M. Deaven, E. Estevez-Aguado, C. J. Guess, J. Gulyás, K. Hatanaka, K. Hirota, M. Honma, D. Ishikawa, A. Krasznahorkay, H. Matsubara, R. Meharchand, F. Molina, H. Nakada, H. Okamura, H. J. Ong, T. Otsuka, G. Perdikakis, B. Rubio, H. Sagawa, P. Sarriguren, C. Scholl, Y. Shimbara, E. J. Stephenson, T. Suzuki, A. Tamii, J. H. Thies, K. Yoshida, R. G. T. Zegers, and J. Zenihiro, Phys. Rev. C **91**, 064316 (2015).
[32] F. Ajzenberg-selove and J. Kelley, Nucl. Phys. A **506**, 1 (1990).
[33] Y. Shimbara, Y. Fujita, T. Adachi, G. P. A. Berg, H. Fujimura, H. Fujita, K. Fujita, K. Hara, K. Y. Hara, K. Hatanaka, J. Kamiya, K. Katori, T. Kawabata, K. Nakanishi, G. Martìnez-Pinedo, N. Sakamoto, Y. Sakemi, Y. Shimizu, Y. Tameshige, M. Uchida, M. Yoshifuku, and M. Yosoi, Phys. Rev. C **86**, 024312 (2012).
[34] H. Fujita (private communication).
[35] J. Comfort, R. Schaeffer, and J. Raynal, DWBA computer code DW81.
[36] S. V. D. Werf, S. Brandenburg, P. Grasduk, W. Sterrenburg, M. Harakeh, M. Greenfield, B. Brown, and M. Fujiwara, Nucl. Phys. A **496**, 305 (1989).
[37] R. Schaeffer, Nucl. Phys. A **164**, 145 (1971).
[38] R. G. T. Zegers, H. Abend, H. Akimune, A. M. van den Berg, H. Fujimura, H. Fujita, Y. Fujita, M. Fujiwara, S. Galès, K. Hara, M. N. Harakeh, T. Ishikawa, T. Kawabata, K. Kawase, T. Mibe, K. Nakanishi, S. Nakayama, H. Toyokawa, M. Uchida, T. Yamagata, K. Yamasaki, and M. Yosoi, Phys. Rev. Lett. **90**, 202501 (2003).
[39] J. Kamiya, K. Hatanaka, T. Adachi, K. Fujita, K. Hara, T. Kawabata, T. Noro, H. Sakaguchi, N. Sakamoto, Y. Sakemi, Y. Shimbara, Y. Shimizu, S. Terashima, M. Uchida, T. Wakasa, Y. Yasuda, H. P. Yoshida, and M. Yosoi, Phys. Rev. C **67**, 064612 (2003).
[40] Y. Fujita, J. Phys.: Conf. Ser. **20**, 107 (2005).
[41] T. Adachi, Y. Fujita, P. von Brentano, G. Berg, C. Fransen, D. D. Frenne, H. Fujita, K. Fujita, K. Hatanaka, M. Honma, E. Jacobs, J. Kamiya, K. Kawase, T. Mizusaki, K. Nakanishi, A. Negret, T. Otsuka, N. Pietralla, L. Popescu, Y. Sakemi, Y. Shimbara, Y. Shimizu, Y. Tameshige, A. Tamii, M. Uchida, T. Wakasa, M. Yosoi, and K. Zell, Nucl. Phys. A **788**, 70 (2007).
[42] E.-W. Grewe, C. Bäumer, H. Dohmann, D. Frekers, M. N. Harakeh, S. Hollstein, H. Johansson, K. Langanke, G. Martínez-Pinedo, F. Nowacki, I. Petermann, L. Popescu, S. Rakers, D. Savran, K. Sieja, H. Simon, J. H. Thies, A. M. van den Berg, H. J. Wörtche, and A. Zilges, Phys. Rev. C **77**, 064303 (2008).
[43] L. Popescu, T. Adachi, G. P. A. Berg, P. von Brentano, D. Frekers, D. De Frenne, K. Fujita, Y. Fujita, E. W. Grewe, M. N. Harakeh, K. Hatanaka, E. Jacobs, K. Nakanishi, A. Negret, Y. Sakemi, Y. Shimbara, Y. Shimizu, Y. Tameshige, A. Tamii, M. Uchida, H. J. Wörtche, and M. Yosoi, Phys. Rev. C **79**, 064312 (2009).

Correction: Spacing errors appeared around the term B(GT) during the production cycle and have been fixed.